Renewable Energy 177 (2021) 268–279

Contents lists available at ScienceDirect

Renewable Energy

journal homepage: www.elsevier.com/locate/renene

Solar and biomass hybridization through hydrothermal carbonization

J.V. Briongos [a, *], S. Taramona [a], J. Gómez-Hernández [a], V. Mulone [b], D. Santana [a]

[a] Universidad Carlos III de Madrid. Escuela Politécnica Superior. Departamento de Ingeniería Térmica y de Fluidos, Avenida de La Universidad 30, 28911, Leganés (Madrid), Spain

[b] Department of Industrial Engineering, University of Rome Tor Vergata, Via Del Politecnico 1, 00133, Rome, Italy

ARTICLE INFO

Article history:
Received 10 February 2021
Received in revised form
20 May 2021
Accepted 24 May 2021
Available online 27 May 2021

Keywords:
Continuous hydrothermal carbonization
Concentrated solar energy
Beam-down solar field
Twin-screw extruders
Organic wastes

ABSTRACT

Hydrothermal carbonization process can transform wet bio-wastes into value-added products. This work aims to hybridize a concentrating solar technology and a biomass reactor for the continuous and sustainable valorization of biomass. The novel technology proposed integrates a linear beam-down solar field with a twin-screw reactor for continuous HTC process. The solar field consists of two reflections that concentrate linearly the sun energy on the ground, where the twin-screw reactor is placed. A mathematical model is proposed to solve both the heat transfer and HTC kinetics for a co-rotating twin-screw reactor. The incoming heat flux from the solar field (8–20 kW/m^2), the reactor length (L/D = 30–60 where D is the diameter) and the rotating velocity of the screw (25–100 rpm) are the main variables used to process the biomass up to the desired severity factor. The simulation results of different lignocellulosic biomasses (loblolly pine, sugarcane bagasse, corn stover and rice husk) are validated against literature data. The developed model shows good agreement with experimental results shown in the literature. The proposed technology foresees hydrochar yields of 64–78% for severity factors of 4.2 and 5.3, respectively, in agreement to the experimental results of 63–70% shown in literature.

1. Introduction

Renewable and sustainable processing of biological wastes into value added products have become an urgent need to deal with an increasing global population, the depletion of natural resources and climate change. Bio-wastes include plants or plant-based wastes, municipal wastes, industrial wastes, animal wastes, and household wastes. Due to its renewability and sustainability, bio-waste could become a viable alternative source of energy. However, processing bio-waste with high moisture by conventional thermal technologies (like slow-pyrolysis, gasification or dry-torrefaction) is not an economical option as a significant amount of energy goes into the drying pretreatment. To solve that, hydrothermal processing could be an attractive technology to process both biomass and municipal organic waste feedstocks as the drying pretreatment is not needed [1–3]. Furthermore, the products obtained could be applied to energy production, soil amendments, super-capacitors and biorefinery processes for a fossil-free economy [4–7], opening a technology pathway towards a circular economy.

Hydrothermal processing is a thermochemical treatment that involves the thermal disintegration of biomass in hot compressed water. Depending on the temperature and pressure conditions, this process transforms biomass into a solid (180–260 °C at 2–10 MPa), a liquid (300–350 °C at 5–20 MPa) or a gas (400–600 °C at 23–45 MPa). Focusing on the hydrothermal process with the lowest energy requirements, i.e. hydrothermal carbonization (HTC), it converts biomass into a value-added product (hydrochar) in the presence of water. The hydrochar produced has a carbon content similar to lignite with mass yields varying from 35% up to 80% [8]. Due to the wide range of nonconventional organic feedstocks that can be converted to value added product, the HTC can be considered as an eco-friendly solution to process many organic wastes [3,9]. The fact that HTC reaction needs water makes it attractive for dealing with a broad range of wet organic feedstocks [2,10–13]. Nevertheless, due to the harsh operational conditions of the process, some challenges regarding kinetics models, heat transfer and reactors models that help to design continuous commercial-scale reactors remain still unanswered.

Literature shows HTC processes running in batch, semi-batch and in continuous reactors with residence times ranging from a few minutes to several hours [9]. The reactor configuration plays a significant role on the reaction kinetics and, therefore, on the

* Corresponding author.
E-mail address: jvilla@ing.uc3m.es (J.V. Briongos).

https://doi.org/10.1016/j.renene.2021.05.146
0960-1481/

product yield and composition because of the high temperature and pressure operational requirements. As pointed by Shen [14], these operational conditions have limited the deployment of commercial HTC application. Indeed, most of the studies reviewed in Ref. [14] used lab-scale pressurized vessels to carry out batch or semi-continuous HTC experiments. For instance, a pilot-scale cylindrical stirred tank reactor with an internal diameter of 24.13 cm was used to process 0.6 kg of corn stover during 240 min [15]. Several lignocellulosic biomasses (corn stover, rice hulls, tahoe mix, switch grass and loblolly pine) were carbonized in a 100 mL Parr bench-top reactor for 5–20 min [16]. Similarly, loblolly pine was processed in a 200 mL Parr reactor for 2, 4 and 6 h with continuous stirring [17].

Several companies have developed commercial HTC reactors. In this line, AVA built an HTC demonstration plant with several reactors working in parallel as a multi-batch system. A continuous stirred-tank reactor that employs a heat exchanger to heat the biomass was introduced by TerraNova Energy to process sewage sludge [18]. Artec used a tubular reactor for continuous HTC [19]. A tube arrangement of 3000 l is proposed for use in small villages or large farms to reduce biomass transport [18]. Ingelia's HTC pilot plant can process continuously 1200–2400 kg of biomass per day [20]. This facility needed a thermal energy of 3600–4900 MJ/kg for heating a vertical pressurized cylinder up to HTC reaction's temperature when processing lignocellulosic biomass waste feedstocks (organic fraction of municipal solid waste, orange peel waste and residues of a pepper plantation). Such energy represented 25–35% of the inherent energy of the obtained hydrochar [21]. A different approach is proposed by Hoekman et al. [22]. A modified twin-screw extruder (TSE) was used to experimentally study a fast HTC process of loblolly pine. The results showed that a TSE can produce hydrochar in higher yields than when using batch HTC processes for similar reaction conditions. In fact, TSE are widely applied in industry as it ensures consistent product performance, there is a good control of the raw material fed and the temperature of each screw element can be monitored [23–27].

Small local biorefinery plants have been proposed to process the biomass near the source minimizing the transportation costs [20,28]. However, HTC is a high energy-demanding process. Therefore, to further enhance the deployment of closed sustainable cycles that transform locally waste biomass feedstocks into valuable products, a renewable energy source is needed. Solar energy appears as an attractive solution although only a few works have combined HTC with solar technologies. Bertolucci et al. [29] proposed the usage of high vacuum solar panels to provide liquid water at 300 °C to the HTC reactor. Bamboo powder was processed in a parabolic trough HTC reactor [30]. This configuration achieved over 180 °C and pressure of 10 bar during 2 h. Ischia et al. [31] coupled a parabolic dish concentrator to a 300 mL reactor. Grape seeds were carbonized at 180, 220 and 250 °C with a residence time of 2 h showing similar results to conventional hydrochars. However, a solar-assisted solution for continuous HTC is still missing. This paper proposes the integration of an HTC twin-screw reactor with a linear-beam down (LBD) solar field to provide a new HTC configuration fully sustainable that can be easily scaled-up. The LBD concentrating solar field allows the concentration of solar energy linearly on heavy receivers placed at the ground level, supplying the energy needed to carry out the HTC process [32,33].

In this work, an HTC process is analytically modelled for a twin-screw reactor coupled to an LBD solar field. This novel layout is proposed to make the HTC process energetically sustainable. An LBD solar field will provide the energy required to preheat the biomass and perform the HTC process in the twin-screw reactor. The proposed twin-screw model solves both the heat transfer and reaction kinetics during HTC process for different lignocellulosic biomasses. The simulation results are validated against published experimental data. As it is shown below, the solar hybridization with the HTC process in produces hydrochar yields of about 64–78% for severity factors of 4.2 and 5.3, respectively, which are in close agreement with the results reported in literature of 63–70% for TSE reactors [34].

2. Materials and methods

This section describes the proposed layout to supply concentrated solar energy to a twin-screw reactor. First, the twin-screw geometry is described. Then, kinetic and axial dispersion models are explained. Finally, the energy balance and the simulated feedstock composition is detailed.

2.1. Solar-assisted HTC in twin-screw reactors

Linear beam-down solar fields are designed to concentrate solar energy on heavy receivers that cannot be installed elevated from the ground. As shown in Fig. 1, LBD solar field consists of two reflections: a primary field of Fresnel heliostats that aims to the focus of a secondary reflector, which is a hyperboloid-shaped heliostat. In this way, solar energy is concentrated linearly on a receiver located at the ground level. LBD sizing has been described in Refs. [32,33]. In this work, the concentrated solar energy (φ_{in}) on half of the barrel's outer surface is 8–20 kW/m^2. Such low energy concentrations ensure a small size of the LBD solar field, promoting its integration with the HTC twin-screw reactor.

2.2. Twin-screw reactor

A co-rotating twin-screw extruder reactor of 25 mm radius is used during the simulation runs in order to illustrate the potential integration of the solar energy with the twin-screw reactor technology for the continuous HTC treatment of the organic feedstock. The geometrical features and the simulation parameters of the two co-rotating screws are respectively shown in Table 1. Only the twin-screw length can change for each biomass.

Previous experience on the use of twin-screw extruders on HTC process [34] report screw speeds of 200–400 rpm, which lead to residence times ranging within 20–30 s. However, as shown later in the results section, the feedstock used in this work cannot be processed at that screw speed when the solar beam-down is used. A low speed of the twin screw (screw speed < 100 rpm) is selected in the solar-assisted HTC process.

2.3. HTC kinetics model in the twin-screw reactor

Hydrothermal carbonization can transform organic wastes into lignite-like products trying to mimic the natural coalification process [11]. First, the dehydration of the organic feedstock occurs followed by polymerization and carbonization reactions. HTC process needs the dissolution of intermediate products and subsequent organic material decomposition in the absence of oxygen. The product yield depends on the reaction severity or severity factor (*SF*). Accordingly, water acts as the reaction medium where the cellulose and hemicellulose present in the organic feedstock hydrolyze to facilitate the homogeneous polymerization reactions of the dissolved components. During the hydrolysis process, the aqueous extractives substances remain dissolved in water and can be subsequently recovered along with the water stream [11,36].

The solid hydrochar is the product where most of the carbon content of the organic feedstock is retained and, although it is a complex process, it can be viewed as a three step process (dehydration of carbohydrates, homogeneous polymerization and

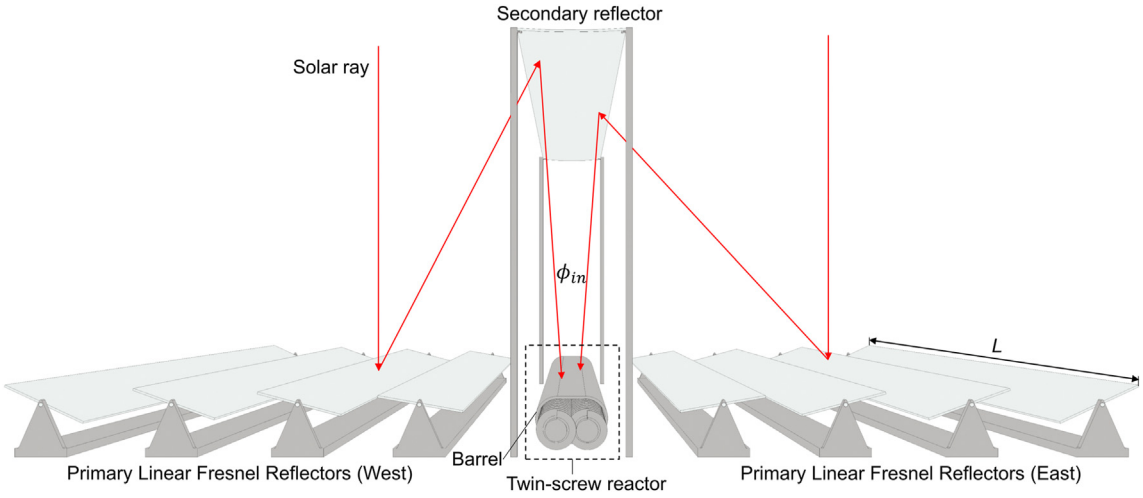

Fig. 1. Linear-beam down solar field for HTC conversion in a twin-screw reactor.

Table 1
Simulation parameters.

Parameter	Value
Screw diameter (D_s) [m]	$50 \cdot 10^{-3}$
Screw pitch length (p_t) [m]	$50 \cdot 10^{-3}$
Screw flight width [m]	$10 \cdot 10^{-3}$
Clearance between screw and barrel (δ) [m]	$1.25 \cdot 10^{-4}$
Screw channel depth (H) [m]	$6.8 \cdot 10^{-3}$
Screw speed (N) [rpm]	25–100
Channel width (w_{ch}) [m]	$15 \cdot 10^{-3}$
Helix angle [rad]	30.82
Overlapping angle (α) [°]	1.055
Center distance [m]	$42.6 \cdot 10^{-3}$
Axial reactor length [m]	3
Axial preheater length [m]	0.25
Number of screw flight [–]	2
Barrel thickness [m]	$20 \cdot 10^{-3}$
Mixture specific heat [kJ/kgK]	4.657
Beam down heat flux (φ_{in}) [kW/m^2]	8–20
Feedstock inlet temperature [°C]	100
Water inlet temperature [°C]	240
Barrel thickness [m]	$20 \cdot 10^{-3}$
High temperature absorptivity coating [–] (Co-WC-Al_2O_3/Al_2O_3) [35]	0.951
Barrel material	AISI4140
Viscosity a high shear rates (η_∞) [Pa s]	$10 \cdot 10^{-12}$
Viscosity at zero shear rate (η_0) [Pa s]	10,000
Solid and wall emissivity [–]	0.8
Relaxation time (λ) [s]	25

carbonization by intermolecular dehydration) [37,38]. The effect of temperature and time on the solid yield is considered by the severity factor, SF (eq. (1) and eq. (2)), to measure the intensity of the treatment [4,9,39,40]:

$$R_0 = \int_0^{\bar{t}} e^{\left(\frac{T(t)-100}{14.75}\right)} dt \quad (1)$$

$$SF = \log_{10} R_0 \quad (2)$$

Where R_0 is the reaction ordinate (min), $\bar{t}$ is the residence time (min) and T is the temperature in [°C]. Consequently, biomass mass flow, reactor geometry and feed density at reacting operating conditions affect such reaction's intensity.

The energy content of the hydrochar increases alongside the severity factor. Besides the solid products, gaseous products and liquid dissolved byproducts are also obtained. The liquid stream is characterized by a lower pH than the water fed initially and it is characterized by a rich organic load. It has been reported in literature that the recirculation of this water can improve both the mass and energy yield of the hydrochar product [38,41]. Moreover, the inorganic components of the organic feedstock are dissolved into the liquid process stream and can be further separated from the solid product. The gaseous products, mainly CO_2, CH_4, CO and H_2, can be separated from the liquid and solid fractions.

To simplify the complex chemistry and reaction scheme characterizing the HTC process, the kinetic models found in literature are based on pseudo-first-order mechanism (hydronium-catalyzed reactions) [40,43]. Moreover, the reaction kinetics are focused on the major organic feedstock structural components, which are the cellulose, the hemicellulose, the lignin, and the aqueous extractives (starch, sugars, proteins and inorganic salts). Furthermore, some additional assumptions help to approximate kinetics. In this work,

the reaction scheme used to model the kinetics of the HTC process assumes a first reaction order for both the hydrolysis of cellulose and hemicellulose components into dissolved intermediates. Later, the products can suffer subsequent polymerization reactions or remain dissolved, Fig. 2. Note that the same kinetics and activation energy are used for both the cellulose and the hemicellulose to simplify the model, since the purpose is to account for the characteristic time of such complex carbonization process. The subsequent carbonization reaction to get hydrochar is described by a higher reaction order, following the approach reported in Ref. [42]. Accordingly, the lignin is assumed to be hydrolyzed in the final step. The reaction kinetics are described as:

$$-r_C = \frac{dC_C}{dt} = -k_C C_C \tag{3}$$

$$-r_H = \frac{dC_H}{dt} = -k_H C_H \tag{4}$$

$$-r_I = \frac{dC_I}{dt} = k_C C_C + k_H C_H - k_{HC} C_I^m - k_G C_I \tag{5}$$

$$-r_{HC} = \frac{dC_{HC}}{dt} = -k_{HC} C_I^m \rightarrow \frac{dC_{HC}}{dt} = -r_{k_H/k_G} k_G C_I^m \tag{6}$$

$$-r_{G-AE} = \frac{dC_{G-AE}}{dt} = -k_G C_I \tag{7}$$

The temperature, which is the main factor controlling the HTC process [4], is provided in terms of the Arrhenius equation (eq. (8)). Table 2 shows the kinetic parameters for the reaction scheme described in Fig. 2.

$$k_i = k_{i,0} e^{-\frac{E_{A,i}}{RT}} \tag{8}$$

Kinetic data is needed to check if the reactive extruder allows short residence times. However, to the best author knowledge, there is a lack of reported literature on kinetic models and kinetic data of HTC screw reactors. Therefore, the purpose of the kinetic model proposed in this research is:

- Check the results shown previously in literature for loblolly pine [34] on the idea of integrating the concentrated solar energy as an energy input to the twin-screw reactor.
- Check if the solar-assisted HTC model could be used with different organic feedstocks. In that line, the model results will be compared against the hydrochar yield obtained for other biomass feedstocks reported in literature [22].

Table 2
Kinetic model parameters [42].

Parameter	Value
$k_{C,0}$, (s^{-1})	$1.89 \cdot 10^{14}\ \bar{t}/\tau_H$
$k_{G,0}$, (s^{-1})	$1.89 \cdot 10^{7}\ \bar{t}/\tau_H$
$k_{H,0}$, (s^{-1})	k_C,
EA_C (kJ mol^{-1})	141
EA_G (kJ mol^{-1})	74.3
EA_H (kJ mol^{-1})	141
k_{HC}, ($kg^{0.53}$ s^{-1}),	$r_{k_{HC}/k_G} \cdot k_G$
m (−)	1.53

Due to absence of kinetic data, some assumptions are necessary in order to solve the conversion scheme shown in Fig. 2 for different feedstocks. Pre-exponential factors from Arrhenius equation shown in Table 2 have been scaled assuming that the residence time of $\bar{t} \sim 48\ h$, which characterizes the results shown in Ref. [42], and the hydraulic characteristic time related to twin-screw reactors, $\tau_H = V_R/V_{Feed}$, are equivalent (i.e. the chemical reaction rate/mass transport by convection ratio match).

The concept of selectivity ($\bar{S}_{HC-GAE}$) is applied to deal with the parallel reactions that produce both *HC* and *G-AE* products (Fig. 2). Accordingly, to solve locally the kinetic model, it is assumed that the local selectivity equals the overall selectivity at any point in the system at the temperature characterizing the reactor outlet at each simulation time. As a result, the ratio between the corresponding

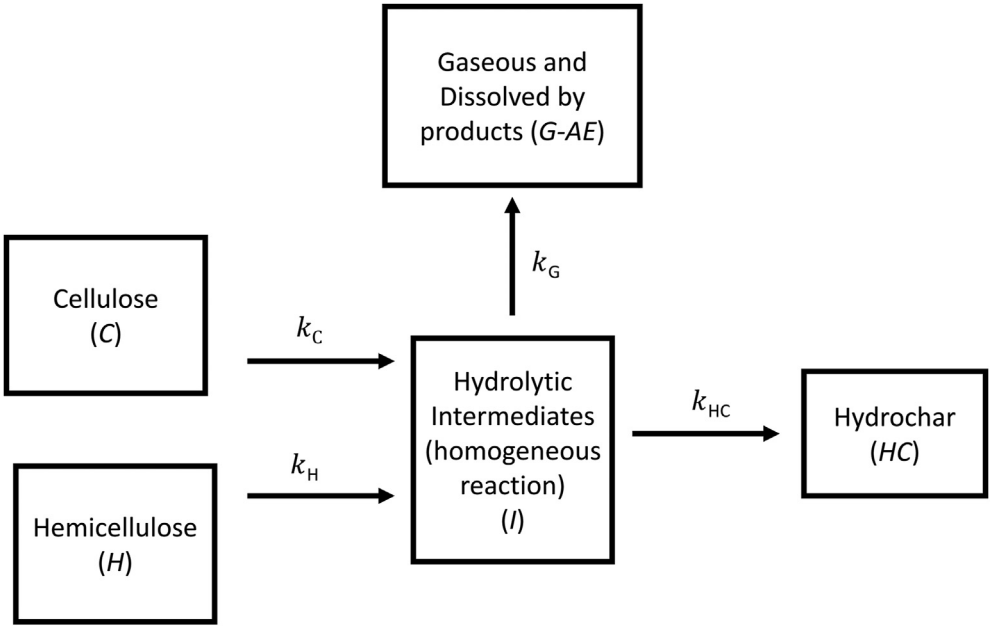

Fig. 2. HTC reaction scheme, based on [42].

kinetic constants is obtained as:

$$\overline{S}_{HC-GAE} = \left(\frac{C_{HC}}{C_{G-AE}}\right)_{\tau_r} = S_{HC-GAE} = \frac{\frac{dC_{HC}}{dt}}{\frac{dC_{G-AE}}{dt}} = \frac{-k_{HC}C_I^m}{-k_G C_I} = \rightarrow r_{k_{HC}/k_G} = \frac{k_{HC}}{k_G} \tag{9}$$

The conversion yield data used to calculate r_{k_H/k_G} is taken from Ref. [22]. As a result, the evolution of the HTC reactions can be calculated through the twin-screw reactor. As it will be shown later, the model accounts for the effect of the severity factor on the hydrochar yield. Accordingly, the model output reflects how the mass yield, given as a percentage of dry feedstock, decreases as severity increases. This result is important because the mass reduction is shown in the energy densification of the corresponding biomass [34].

2.4. Axial dispersion model in the twin-screw reactor

The complex flow patterns of twin-screw extruders provide good mixing and good heat transfer features. However, it is complicated to describe heat and mass transfer coefficients as a function of the twin-screw geometry or as a function of feedstock properties under HTC process conditions [36]. Residence time distributions (RTD) reported in literature for screw extruders present plug flow features that make the axial dispersion model suitable to describe those systems [44–48]. According to that, in order to match the results reported in literature, in this research it is assumed a diffusion-like process along the downward flow stream direction that is superimposed on the ideal plug-flow behavior. The proposed model considers the interaction between the advection mixing, the diffusion and the chemical reaction assuming constant diffusivity of species. As a result, the mass balance for each specie reads as:

$$\frac{\partial C_i}{\partial t} + u_z\frac{\partial C_i}{\partial z} = D_L\frac{\partial^2 C_i}{\partial z^2} + r_i \tag{10}$$

Where u_z is the downward channel-unrolled average velocity, r_i is the reaction rate and D_L represents the dispersion coefficient. Large D_L values involve an inefficient vertical mixing causing a strong longitudinal spreading. It is worth to mention that the reaction rate equals zero for the tracer experiments shown below in the results section. In order to set the average fluid speed, u_z, the C-shape chambers that characterize the intermeshing twin-screw flow geometry are simplified to unrolled rectangle channels. The unrolled length is divided into pieces, $L_i = R(2\pi - \alpha)/\cos(\theta)$ corresponding to the screw C-channel length. In this model, the channel depth is assumed to be small compared to the width, so only the direction towards the end of the channel is considered. According to that, the momentum equation can be written as:

$$\frac{dP}{dz} = \eta\frac{d^2 v_z}{dy^2} \tag{11}$$

Where P is the local pressure in the direction towards the end of the channel, v_z is the velocity in the channel direction and the viscosity (η) is given by the Carreau model [49]:

$$\eta = \eta_\infty + (\eta_0 - \eta_\infty)\left(1 + (\lambda\dot{\gamma})^2\right)^{\frac{n-1}{2}} \tag{12}$$

where $n = 0.3$ is the power index, η_∞ is the viscosity a high shear rates and η_0 is the viscosity at zero shear rate,λ is the relaxation time and $\dot{\gamma}$ is the shear rate. Moreover, the pressure drop will be affected by the filling degree of the channel (ε), which is given by:

$$\varepsilon = \frac{Q_a}{Q_{th}} \tag{13}$$

Where Q_a refers to the actual volumetric feed flow rate and Q_{th} accounts for the theoretical throughput. The mean value is used in the model equations to account for the corresponding advection terms.

Reactive extruders for HTC reactions should guarantee a good mixing to provide the homogeneous conditions that maximize the reaction yield. A priori, HTC processes might present dispersive and longitudinal mixing, and therefore, both mechanisms may affect the reaction yield. In this work, dispersive mixing is neglected as there is a lack of information in literature regarding HTC twin-screw dispersive studies. This means that the slurry mixture is assumed to be well-mixed in the radial direction. Consequently, both the water and the reacting polymer phase mixture are assumed to behave as a slurry mixture.

The axial dispersion influence will be investigated using the residence time distribution. An ideal pulse of tracer of 10 s will be simulated at the reactor inlet. The resulting age distribution function, E_t (eq. (14)), which represents the retention time of the material leaving the extruder, is expressed in dimensionless form (E_θ, eq. (16)) as a function of the mean residence time ($\bar{t}$) and the dispersion number (D_L/uL) that characterizes the distribution [50].

$$E_t = \frac{C(t)}{\int_0^\infty C(t)dt} \tag{14}$$

$$\bar{t} = \int_0^\infty tE_t dt \tag{15}$$

$$E_\theta = \frac{1}{\sqrt{4\pi(D_L/uL)\theta}}e^{\left[-\frac{(1-\theta)^2}{4\theta(D_L/uL)}\right]} \tag{16}$$

$$\sigma_\theta^2 = \frac{\sigma_t^2}{\bar{t}^2} = 2\frac{D_L}{uL} + 8\left(\frac{D_L}{uL}\right)^2 \tag{17}$$

Where $\boldsymbol{C}(\boldsymbol{t})$ is the tracer concentration, $\boldsymbol{\theta}$ is the dimensionless time, $\boldsymbol{\theta} = \boldsymbol{t}/\bar{\boldsymbol{t}}$, $\boldsymbol{D_L}$ is the axial dispersion coefficient, L is the axial reactor length, and $\boldsymbol{\sigma_t^2}$ is the variance of the RTD curve.

2.5. Energy balance of the twin-screw reactor

The unrolled axial formulation is followed to solve the energy flow in the extruder. Therefore, the heat transfer is solved along the twin screw extruder unrolled channel:

$$\rho c_p\left(\frac{\partial T_i}{\partial t} + u_z\frac{\partial T_i}{\partial z}\right) = \eta\dot{\gamma}^2 + Q_{Wall} + r_i\Delta H_r \tag{18}$$

Where c_p is the specific heat of reacting mixture, ρ is the density of the reacting mixture, u_z is the average velocity profile in the down chamber direction. Eq. (18) considers the temperature rise of the reacting mixture, T_i, given by the viscous friction component, where the shear rate in the extruder channel can be approximated by $\dot{\gamma} = \pi D_s N/60H$ [51] or from the velocity profiles characterizing the extruder channel, the wall heat transfer (convection heat

transfer and radiation), the advection transport term and the reaction term. Regarding the reaction term, $r_i \Delta H_r$, it has been reported in literature that HTC reaction exhibits small exothermicity [52]. According to that, in this work, the heat of reaction is neglected adopting a conservative approach in terms of energy input needs.

The heat transfer coefficient of the convection term is given by Todd's correlation [53,54]:

$$Nu = \frac{h_T D_s}{k} = 0,94 \left(\frac{D_s^2 N \rho}{\eta} \right)^{0,28} \left(\frac{c_p \eta}{k} \right)^{0,33} \left(\frac{\eta_0}{\eta} \right)^{0,14} \quad (19)$$

Where h_T is the convection heat transfer coefficient, D_s, is the screw diameter, k reacting mixture conductivity, N is the screw speed, c_p is the specific heat of the reacting mixture, ρ is the density of the reacting mixture, η is the viscosity, and η_0 is the viscosity at zero shear rate.

Regarding the radiation heat transfer term, the screw channel is assumed to behave as a two-dimensional channel that significative extends in the flow directions. In this way, Hottel's crossed-string method [55] can be used to calculate the radiant heat interchanged between the inner surface of the barrel and the reacting mixture. According to that, the radiation problem is solved as the radiative exchange between two gray surfaces. In the end, the wall heat transfer term shown in eq. (18) is the result of both convection and radiation terms.

Finally, the energy balance at the outer barrel surface includes the heat radiation provided by the beam down receptor (φ_{in}), convection ($Q''_{conv,loss}$) and radiation ($Q''_{r,out}$) losses.

$$Q''_{surf} = \varphi_{in} \alpha_{coat} - \left(Q''_{r,out} + Q''_{conv,loss} + Q''_{conv,\ fluid} \right) \quad (20)$$

The model equations are solved with the following assumptions:

1. The transverse diffusion is assumed to be a fast process, consequently the longitudinal diffusion due to the shear effect obeys the Fickian's diffusion law.
2. Only the top half of the barrel surface is exposed to the beam down radiation.
3. Concentrated radiation is uniformly distributed on the top half of the barrel surface.
4. The viscous friction component is converted directly into heat by internal friction that is utilized to heat the reacting mixture.
5. The concentrated solar energy from the LBD solar field is transferred from the wall to the reacting mixture by convection and radiation heat transfer mechanisms.
6. The hot water and the organic feedstock are mixed adiabatically at the inlet of the reactor.
7. The hot water feed and the reacting polymer phase mixture are assumed to be a well-mixed slurry.
8. Leakage flows are not considered as the screw is divided into “isolated areas”.
9. The pressure profile is not considered during the reaction and, in contrast, a pressure of 100 bar is assumed to characterize the reaction zone.

2.6. Simulated feedstocks

In the simulation runs, biomass and water are fed to the twin-screw reactor inlet at a temperature of 100 °C. The kinetic mechanisms described above are solved for the biomass feedstocks described in Table 3. Water properties are calculated using CoolProp library [56].

3. Results and discussion

The HTC model proposed in this work is based on two main assumptions: (i) the local selectivity is similar to the overall selectivity in the twin-screw reactor, and (ii) each screw element is simplified to be isolated, which it is assumed to feed, mix, pump, convey the slurry and eventually melt the corresponding hydrochar product. In this section, we first determine the relevance of the main parameters of TSE-LBD approach (the reactor length, L/D, the concentrated solar energy φ_{in} and the screw rotational speed, N) on the severity factor. Then, the model is validated optimizing the parameters to obtain the target value of the severity factor. Later, the transient response of the model kinetics is studied. Finally, the dispersion influence is considered to discuss the mixing features of the twin-screw reactor.

3.1. Model performance

The model is analyzed changing the three main input parameters:

(i) Twin-screw reactor length, $L/D = 30 - 60$.
(ii) Screw rotating velocity, $N = 25 - 100\ rpm$.
(iii) Concentrated solar energy from the LBD solar field, $\varphi_{in} = 8.5 - 20\ kW/m^2$.

The rest of the geometric characteristics of the twin-screw reactor are fixed in the model, as shown in Table 1. Fig. 3 studies the model performance as a function of the three main variables. In this figure, the values of the three variables are chosen to obtain high severity factors. Therefore, the severity factor is the independent variable, so to obtain a certain value of the severity factor, the reactor length (Fig. 3-a), beam-down heat flux (Fig. 3-b) and rotating speed (Fig. 3-c) can be selected to obtain a LBD-TSE reactor design. Note that the results shown in Fig. 3 are not optimized. Indeed, these design solutions are reported here as design examples of twin-screw reactors able to reach high severity factors. Appendix 1 shows the residence times and *HC* conversion yields for the design examples reported.

The three variables are combined to design each twin-screw reactor up to the desired severity factor. Both the reactor length and the rotating screw velocity are used to control the residence time mechanically, while the incoming solar heat flux influences the HTC transformation. For instance, to obtain a severity factor of 6 for loblolly pine, a long reactor of $L/D = 60$ (Fig. 3-a) coupled to a LBD solar field capable to concentrate $\varphi_{in} = 16\ kW/m^2$ (Fig. 3-b), at a rotating screw speed of $N = 25\ rpm$ (Fig. 3-c) is needed. Therefore, high severity factors are obtained when the residence time increases, which is shown in long screws at low rotating speeds, and the heat flux is high. Furthermore, it is worth to mention that the screw velocity is maintained at 25 rpm for loblolly pine and sugarcane bagasse to obtain high severity factors, as shown in Fig. 3-c.

The three main parameters shown in Fig. 3 significantly modify the HTC process outcome. Therefore, it is mandatory to select them as a function of the biomass type and the severity factor to be obtained.

3.2. Model validation

Fig. 4 shows the mass yield, calculated as a percentage of the starting dry feedstock mass, predicted by the model (solid line) and the experimental results reported in literature for different severity factors and different feedstocks. Note that the experimental results

Table 3
Organic feedstocks.

	Cellulose (%)	Hemicellulose (%)	Lignin (%)	Ash + Extractive (%)	Moisture (%)	Bulk density (kg/m^3)	Water/Biomass ratio	Feed rate, $\dot{m}_F$ (kg/h)
Sugarcane bagasse	48.45	29.92	17.12	4.51	53	590	3.5	7.5
Loblolly pine	55.4	11.5	30	3.1	53	513	3.5	7.5
Corn Stover	34.5	27.7	17.8	20	8	131/156	3.5	7.5
Rice husk	39.8	14.9	11.3	34	7.27	107	3.5	7.5

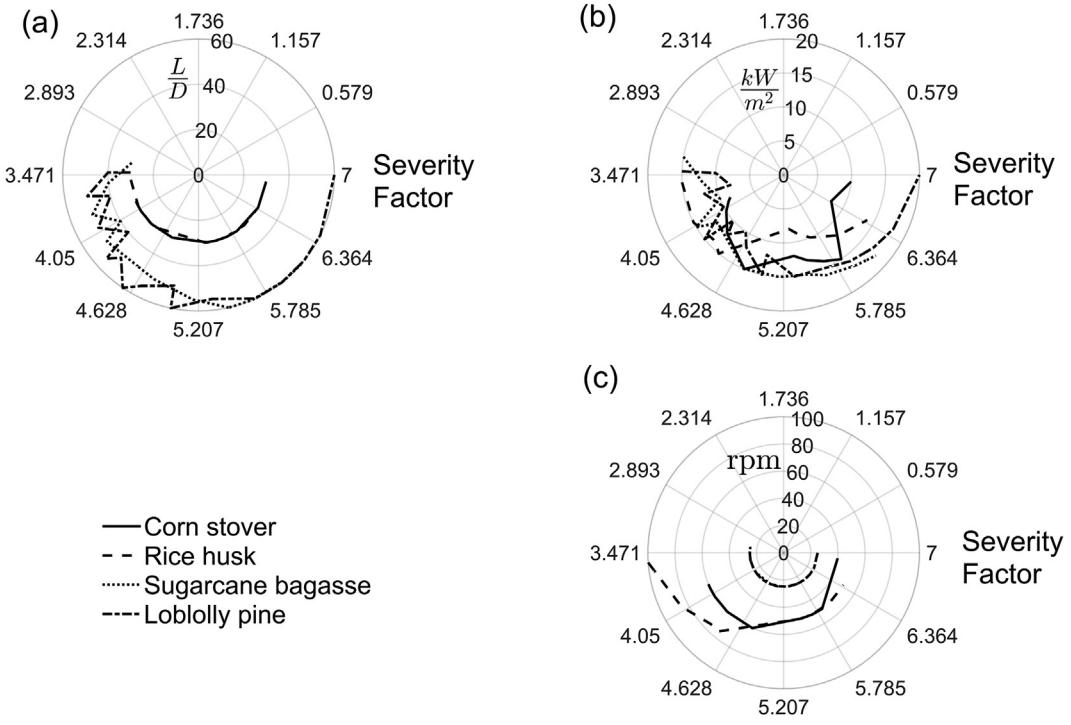

Fig. 3. Severity factors simulation conditions: a) *L/D* ratio, b) linear beam-down heat flux, c) rotating screw velocity.

of the twin-screw reactor operating with loblolly pine are marked in red [34]. As commented before, L/D, N, and φ_{in} were selected to approximate the simulation results of the model to the experimental results shown in literature.

The simulation results are in good agreement with the data reported in Ref. [34] for loblolly pine (Fig. 4-a), sugarcane bagasse (Fig. 4-b) and rice husk (Fig. 4-c). Indeed, experimental results reported in literature [16,22,39], which were obtained using pressurized vessels, are close to the model simulations, which considers a twin-screw reactor. This suggests that the mass yield and severity factor are strongly correlated regardless of the reactor used.

Regarding the experimental results reported in Ref. [34] for a twin-screw reactor, there is a good agreement with the model. Moreover, in the case of loblolly pine feedstock (Fig. 4-a), there is only a small difference between the model and the data. Such a difference can be explained due to the axial dispersion process, as studied in detail below.

On the contrary, when employing corn stover feedstock (Fig. 4-d), the reported data is scattered [15,16,22,39,57]. Two different bulk densities have been simulated (solid and dashed lines). The model only approaches the experimental reported data for severity factors above 6. Even the data of [22], which is used to solve the kinetic model proposed in this work, is far from the simulation results for severity factors below 6. Corn stover fractions (stalks, leaves, tassel, husk, and cob) exhibit a significant variation in mass of biomass moisture and composition. Moreover, these parameters seem to be affected by growing seasons, planting density and corn variety. Consequently, it is hard to find representative samples of corn stover for design purposes. As a result, some design parameters used by the model, such as the bulk density, are affected by the aforementioned factors and therefore it may explain why simulation results are far from the experimental results reported in literature. This result points out the critical need of kinetic data to design and guide continuous HTC reactors.

3.3. TSE reactor analysis

Once the kinetics have been validated, the reactor performance is studied considering loblolly pine under a heat flux of $\varphi_{in} = 10\ kW/m^2$, a reactor length of $L/D = 60$ and a rotating velocity of $N = 25\ rpm$. A severity factor of 4.8 is obtained for these design conditions.

Fig. 5 shows the products obtained at the outlet of the twin-screw reactor as a function of time since the start of the experiment. Left y-axis shows the product yield as a percentage of the starting dry feedstock mass, while the right y-axis presents the temperature evolution of the products. The results of both variables are shown at the reactor outlet. Different time intervals are identified and numbered throughout the simulation time.

As aforementioned, biomass and water are continuously fed at 100 °C at the inlet of the reactor, while the heat flux from the solar field is maintained at $10\ kW/m^2$ during the whole simulation.

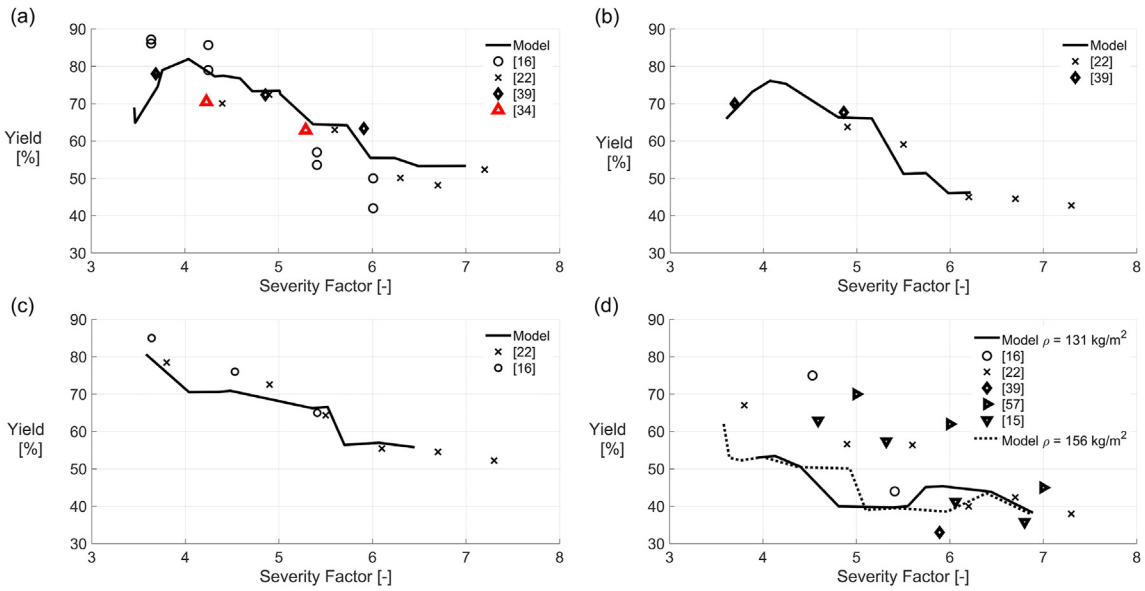

Fig. 4. Hydrochar yield as a function of the severity factor, the lines show the output of the proposed twin-screw reactor: (a) loblolly pine, (b) sugarcane bagasse, (c) rice husk, (d) corn stover.

Interval time 1 represents the time that the biomass and water mixture need to increase their temperature from the initial 100 °C until reaching the reaction temperature of 150 °C at the outlet of the reactor. Thus, around 500 s are needed to obtain some reaction products at the twin-screw output. The biomass and water mixture leave the twin-screw reactor without performing the HTC process for 715 s. Such period of time is needed to heat up the biomass and water mixture until a significative start of the HTC process. Note that the proportion of hydrochar produced is very low due to the low temperatures. Interval 2 shows the starting of the HTC process, which is characterized by a fast conversion of the soluble fraction of organics and lignin content to hydrochar. There is a significative increase of the hydrochar yield during this period due to the increase of the slurry temperature. Interval 3 shows the hemicellulose and cellulose degradation of biomass, in a temperature range from 160 °C to 200 °C, when hemicellulose and cellulose hydrolysis takes place. Finally, interval 4 (200–226 °C) is characterized by decarboxylation and polymerization reactions. The reaction pathway shown in Fig. 5 agrees with HTC kinetics reported in literature [38,58], and with the previous results shown in Fig. 4. Therefore, these results support the kinetic model approach followed in this research.

Similar conditions used to compute Fig. 5 (loblolly pine, $\varphi_{in} = 10\ kW/m^2$, $L/D = 60$, $N = 25\ rpm$, $SF = 4.8$) are analyzed at steady state in Fig. 6. As can be seen in Fig. 6-a, the temperature profile that characterizes the slurry is roughly linear. Furthermore, the outer

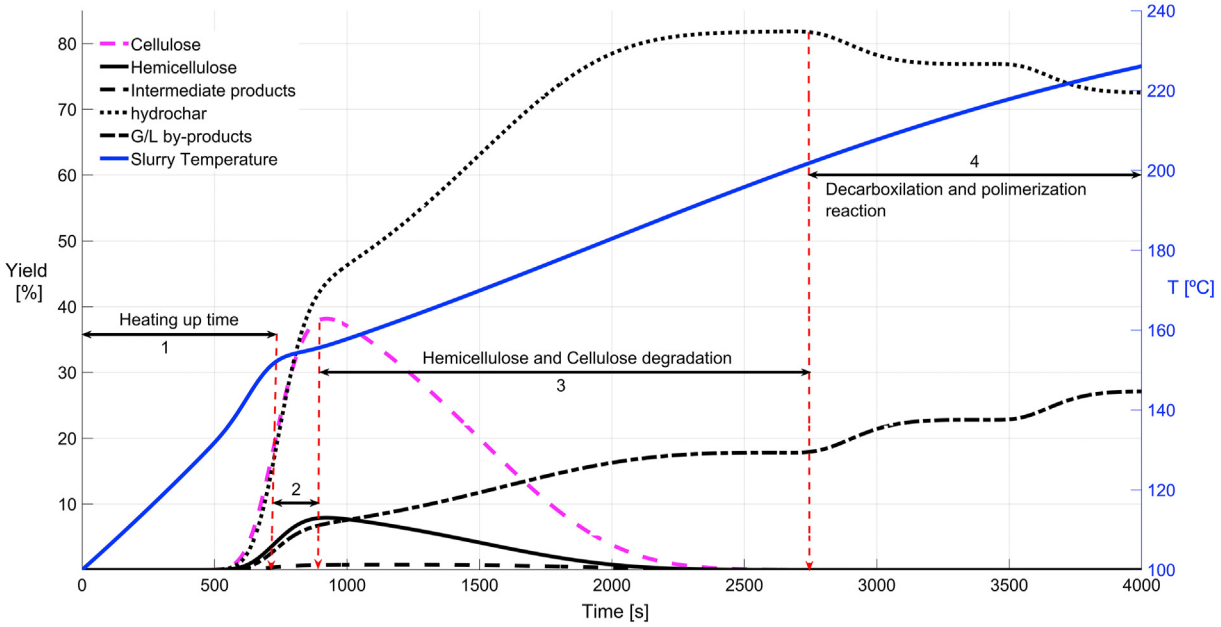

Fig. 5. Transient evolution of the products obtained at the outlet of the twin-screw reactor during the hydrothermal carbonization of loblolly pine, $\varphi_{in} = 10\ kW/m^2$, $L/D = 60$, $N = 25\ rpm$, $SF = 4.8$. (composition given as a percentage of the starting dry feedstock mass).

barrel surface is lower than the maximum temperature of 600 °C allowed by the coating used [35].

Fig. 6-b/c study the model deviation from plug-flow injecting a tracer. Both the dimension and dimensionless response show a symmetrical behavior characteristic of small dispersion numbers. Although the simulation runs have been carried out considering a small axial deviation from plug-flow, there are RTD results in literature that deviates from plug-flow operation [44–46,48]. Consequently, it is worth to study the effect of nonideal plug-flow deviation on the model results.

3.4. Dispersion influence

Axial mixing influence through the screw channel is investigated analyzing the residence time distribution. RTD simulation runs are carried out to determine the residence time as well as the dispersion number that might characterize the twin-screw reactor when operating under different dispersion conditions. In this line, and ideal pulse of tracer of 10 s is introduced at the reactor inlet.

Different runs have been conducted for dispersion numbers $D_L/uL = 0.001 - 0.19$ to explore the dispersion effect on the reactor performance. Accordingly, the residence time is calculated from the tracer curve. Fig. 7 shows the dimensionless response curve for the twin-screw extruder operating for loblolly pine, $\varphi_{in} = 10\ kW/m^2$, $L/D = 60$, $N = 25\ rpm$, $SF = 4.8$, and characterized by different dispersion numbers (D_L/uL).

As expected, it can be observed that the average residence time that characterizes the reactor decreases when increasing the dispersion number. The effect of broadening the response curve can be observed in Fig. 7. Large dispersion numbers imply a large deviation from plug-flow and therefore, the severity factor measured as a function of the average residence time fails as a controlling parameter of the hydrochar conversion. The red arrow points out the values of the dispersion number that cause the model failure when comparing with literature results, which is studied in Fig. 8.

As shown in Fig. 8, there is a deviation on the operational line above $D_L/uL > 0.1$ (dashed line) from which the hydrochar yield largely deviates from the reported literature data and consequently, the axial dispersion model fails in predicting the performance of the systems largely deviated from plug-flow. Therefore, the axial dispersion plays a significant role on the design of twin-screw reactors for HTC.

4. Conclusions

This work proposes a model of a novel technology that can carry out the hydrothermal carbonization of biomass continuously and sustainably. To achieve that, this technology combines a twin-screw reactor with a linear beam-down solar field, which supplies the energy required to perform the HTC process.

The three main variables, twin-screw reactor length, screw rotating velocity and concentrated solar energy from the LBD solar field, determine the HTC product yield and severity factor. The proper selection of these variables leads to high severity factors, which are close to the literature data. In this way, the proposed model approaches the experimental results of the twin-screw facility shown in Ref. [34] when considering a low deviation from plug-flow.

The reaction scheme followed in this research explain the previous results shown in literature in terms of hydrochar yield and reaction severity for several biomasses, even for HTC processes carried out in reactors different to a twin-screw. Moreover, the study of the transient evolution of the hydrothermal carbonization products obtained at the reactor outlet is consistent with the HTC reaction mechanisms reported in literature. Furthermore, the axial dispersion influences the model outcome, which shows good agreement with literature results for plug-flow behavior when $D_L/uL < 0.1$.

According to the model, low rotating screw speeds (screw speed < 100 rpm) are appropriate for the HTC hybridization with concentrated solar energy. The different reactor performances observed for the four organic feedstocks analyzed points out the critical role that the biomass composition will play on the twin-screw reactor performance. Therefore, the twin-screw reactor should be carefully designed to optimize the processing capabilities. In this regard, future works may optimize the twin-screw

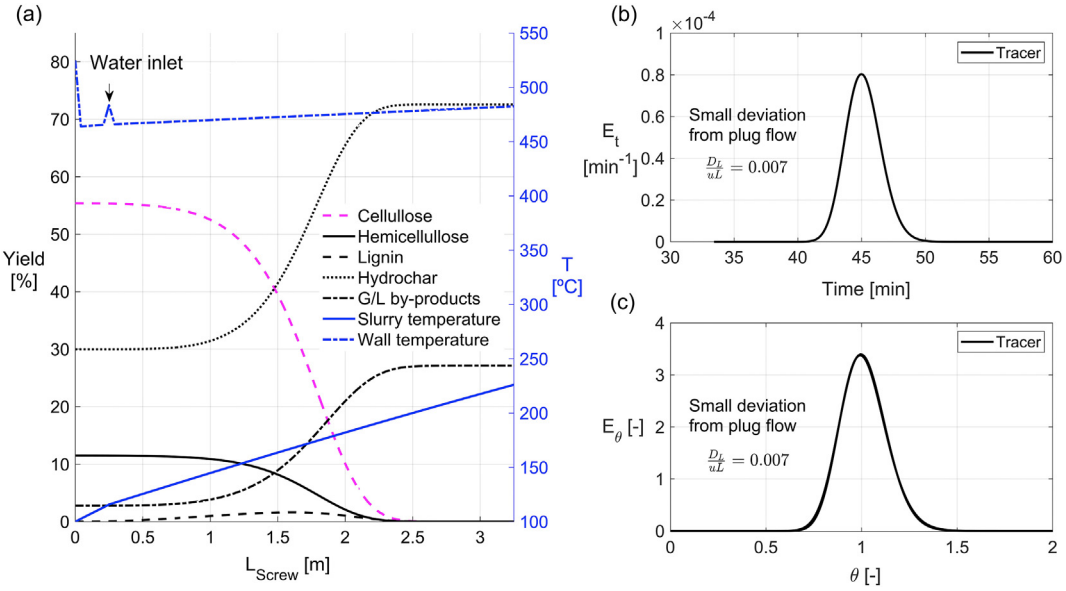

Fig. 6. Stationary results for loblolly pine, $\varphi_{in} = 10\ kW/m^2$, $L/D = 60$, $N = 25\ rpm$, $SF = 4.8$: (a) mass concentration profile calculated as a percentage of the starting dry feedstock mass, (b) dimension response E_t curve, (c) dimensionless response E_θ curve.

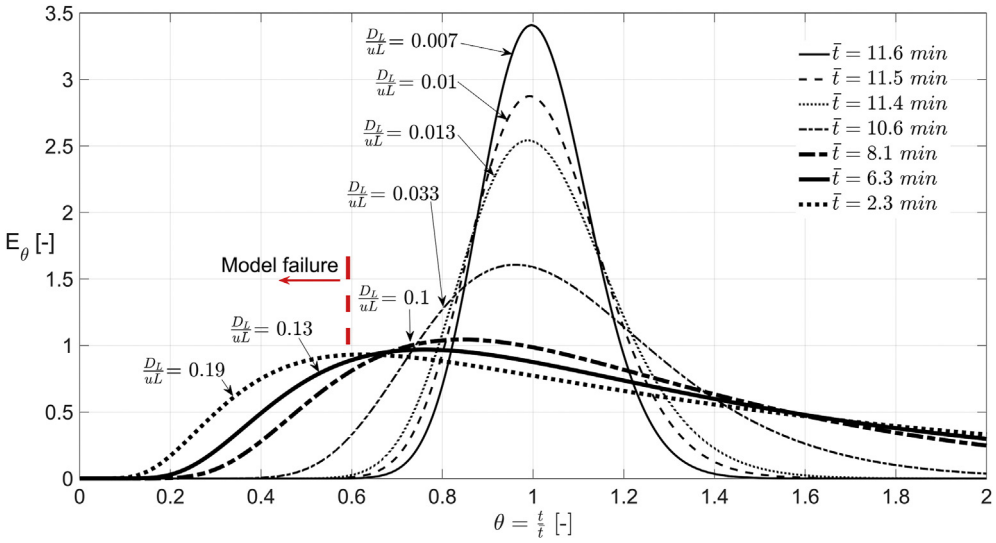

Fig. 7. Dimensionless response curves for loblolly pine, $\varphi_{in} = 10\ kW/m^2$, $L/D = 60$, $N = 25\ rpm$, $SF = 4.8$, operating at different dispersion numbers, D_L/uL.

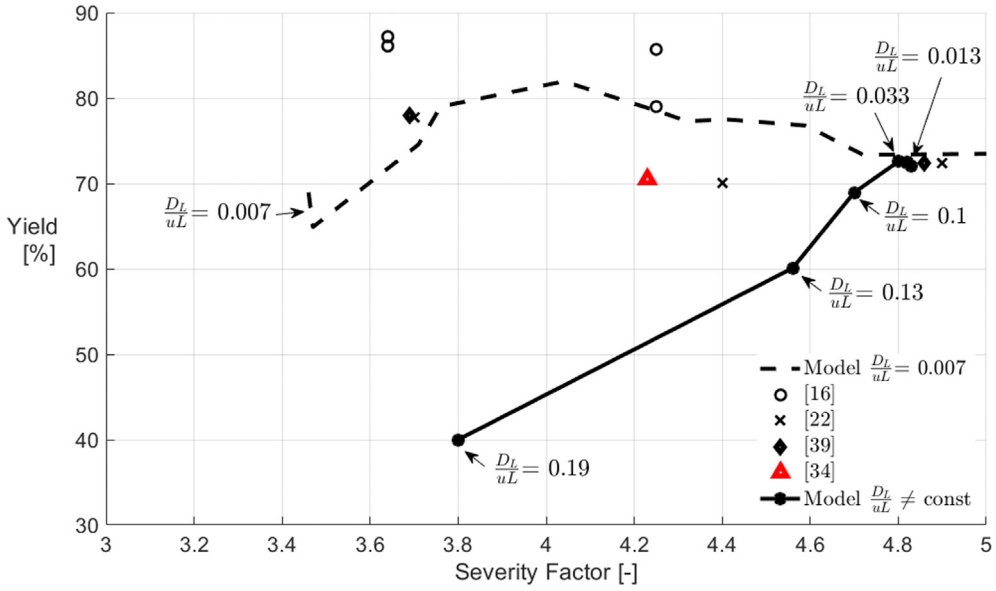

Fig. 8. Hydrochar yield of loblolly pine as a function of the severity factor. The solid line shows the twin-screw model output for different dispersion numbers.

designs for low values of the incoming heat flux from the solar field, in order to reduce both the reactor and the solar field lengths, and thus, minimizing the costs of the TSE-LBD technology.

CRediT authorship contribution statement

J.V. Briongos: Conceptualization, Methodology, Software, Writing – original draft, Investigation. **S. Taramona:** Visualization, Investigation. **J. Gómez-Hernández:** Visualization, Writing – original draft, Investigation. **V. Mulone:** Writing- Reviewing and Editing. **D. Santana:** Supervision.

Declaration of competing interest

The authors declare that they have no known competing financial interests or personal relationships that could have appeared to influence the work reported in this paper.

Acknowledgements

The authors wish to thank “Comunidad de Madrid” for its support to the ACES2030-CM Project (S2018/EMT-4319) through the Program of R&D activities between research groups in Technologies 2018, co-financed by European Structural Funds. Also, the authors wish to thank the research project INTECSOLARIS-CM-UC3M, funded by the call “Programa de apoyo a la realización de proyectos interdisciplinares de I + D para jóvenes investigadores de la Universidad Carlos III de Madrid 2019–2020” under the frame of the “Convenio Plurianual Comunidad de Madrid - Universidad Carlos III de Madrid”.

Appendix

Model simulation results are included in the following tables for loblolly pine, corn stover, sugarcane bagasse and rice husk.

Table A.1
Loblolly pine.

N [rpm]	Residence time [s]	SF [−]	φ_{in} [kW/m^2]	L/D [−]	Mass yield [%]
25	347	3,46	15	30	69%
25	464	3,47	10	40	64,89%
25	581	3,71	8	50	74,57%
25	464	3,76	12	40	79,00%
25	581	4,04	10	50	81,96%
25	464	4,26	15	40	78,36%
25	640	4,32	10	55	77,29%
25	581	4,41	12	50	77,50%
25	696	4,59	10	60	76,78%
25	640	4,72	12	55	73,35%
25	581	5,01	15	50	73,48%
25	696	5,02	12	60	72,56%
25	640	5,37	15	55	64,48%
25	696	5,73	15	60	64,22%
25	696	5,98	16	60	55,50%
25	696	6,24	17	60	55,46%
25	696	6,49	18	60	53,31%
25	696	7,00	20	60	53,34%

Table A.2
Corn stover ($\rho = 131\ kg/m^3$).

N [rpm]	Residence time [s]	SF [−]	φ_{in} [kW/m^2]	L/D [−]	Mass yield [%]
60	133	3,94	8.5	30	53%
60	133	4	9	30	53,17%
60	133	4,13	10	30	53,45%
60	133	4,13	10	30	53,45%
60	133	4,4	12	30	50,59%
60	133	4,81	15	30	39,99%
50	191	5,39	12	30	39,70%
50	191	5,55	13	30	40,01%
50	191	5,74	14	30	45,11%
50	191	5,92	15	30	45,37%
40	337	6,44	8	30	43,88%
40	337	6,89	10	30	38,27%

Table A.3
Corn stover ($\rho = 156\ kg/m^3$).

N [rpm]	Residence time [s]	SF [−]	φ_{in} [kW/m^2]	L/D [−]	Mass yield [%]
60	133	3,64	9	60	53,02%
60	133	3,76	10	60	52,26%
60	133	3,76	10	60	52,26%
60	133	4	12	60	53,18%
60	133	4,38	15	60	50,46%
50	191	4,93	12	50	50,12%
50	191	5,1	13	50	39,00%
50	191	5,26	14	50	39,27%
50	191	5,43	15	50	39,54%
40	337	5,97	8	40	38,56%
40	337	6,39	10	40	43,49%
40	337	6,86	12	40	37,98%

Table A.4
Sugarcane bagasse.

N [rpm]	Residence time [s]	SF [−]	φ_{in} [kW/m^2]	L/D [−]	Mass yield [%]
25	346	3,3	15	30	51,55%
25	452	3,6	12	40	65,98%
25	567	3,88	10	50	73,20%
25	452	4,07	15	40	76,14%
25	567	4,24	12	50	75,33%
25	567	4,8	15	50	66,36%
25	624	5,16	15	55	66,07%
25	681	5,5	15	60	51,22%
25	681	5,74	16	60	51,41%
25	681	5,98	17	60	46,07%
25	681	6,22	18	60	46,21%

Table A.5
Rice husk.

N [rpm]	Residence time [s]	SF [−]	φ_{in} [kW/m^2]	L/D [−]	Mass yield [%]
100	61,6	3,58	15	30	80,66%
85	77,4	4,04	15	30	70,52%
75	93,6	4,36	14	30	70,58%
75	93,6	4,48	15	30	70,91%
50	196,6	5,36	8	30	66,22%
50	196,6	5,52	9	30	66,60%
50	196,6	5,7	10	30	56,43%
50	196,6	6,07	12	30	56,99%
50	196,6	6,45	14	30	55,80%

References

[1] S. Kang, X. Li, J. Fan, J. Chang, Solid fuel production by hydrothermal carbonization of black liquor, Bioresour. Technol. 110 (2012) 715–718, doi.org/10.1016/j.biortech.2012.01.093.

[2] P. Zhao, Y. Shen, S. Ge, Z. Chen, K. Yoshikawa, Clean solid biofuel production from high moisture content waste biomass employing hydrothermal treatment, Appl. Energy 131 (2014) 345–367, https://doi.org/10.1016/j.apenergy.2014.06.038.

[3] R.V.P. Antero, A.C.F. Alves, S.B. de Oliveira, S.A. Ojala, S.S. Brum, Challenges and alternatives for the adequacy of hydrothermal carbonization of lignocellulosic biomass in cleaner production systems: a review, J. Clean. Prod. 252 (2020), https://doi.org/10.1016/j.jclepro.2019.119899.

[4] M. Heidari, A. Dutta, B. Acharya, S. Mahmud, A review of the current knowledge and challenges of hydrothermal carbonization for biomass conversion, J. Energy Inst. 92 (2019) 1779–1799, https://doi.org/10.1016/j.joei.2018.12.003.

[5] H.S. Kambo, A. Dutta, A comparative review of biochar and hydrochar in terms of production, physico-chemical properties and applications, Renew. Sustain. Energy Rev. 45 (2015) 359–378, doi.org/10.1016/j.rser.2015.01.050.

[6] F. Fornes, R.M. Belda, A. Lidón, Analysis of two biochars and one hydrochar from different feedstock: focus set on environmental, nutritional and horticultural considerations, J. Clean. Prod. 86 (2015) 40–48, https://doi.org/10.1016/j.jclepro.2014.08.057.

[7] H.B. Sharma, B.K. Dubey, Binderless fuel pellets from hydrothermal carbonization of municipal yard waste: effect of severity factor on the hydrochar pellets properties, J. Clean. Prod. 277 (2020), https://doi.org/10.1016/j.jclepro.2020.124295.

[8] M. Kumar, A. Olajire Oyedun, A. Kumar, A review on the current status of various hydrothermal technologies on biomass feedstock, Renew. Sustain. Energy Rev. 81 (2018) 1742–1770, https://doi.org/10.1016/j.rser.2017.05.270.

[9] F. Ahmad, E.L. Silva, M.B.A. Varesche, Hydrothermal processing of biomass for anaerobic digestion – a review, Renew. Sustain. Energy Rev. 98 (2018) 108–124, https://doi.org/10.1016/j.rser.2018.09.008.

[10] E. Danso-Boateng, R.G. Holdich, S.J. Martin, G. Shama, A.D. Wheatley, Process energetics for the hydrothermal carbonisation of human faecal wastes, Energy Convers. Manag. 105 (2015) 1115–1124, https://doi.org/10.1016/j.enconman.2015.08.064.

[11] W. Xiang, X. Zhang, J. Chen, W. Zou, F. He, X. Hu, D.C.W. Tsang, Y.S. Ok, B. Gao, Biochar technology in wastewater treatment: a critical review, Chemosphere 252 (2020), https://doi.org/10.1016/j.chemosphere.2020.126539.

[12] Q. Chu, T. Lyu, L. Xue, L. Yang, Y. Feng, Z. Sha, B. Yue, R.J.G. Mortimer, M. Cooper, G. Pan, Hydrothermal carbonization of microalgae for phosphorus recycling from wastewater to crop-soil systems as slow-release fertilizers, J. Clean. Prod. (2020), https://doi.org/10.1016/j.jclepro.2020.124627.

[13] R. Yahav Spitzer, V. Mau, A. Gross, Using hydrothermal carbonization for sustainable treatment and reuse of human excreta, J. Clean. Prod. 205 (2018) 955–963, https://doi.org/10.1016/j.jclepro.2018.09.126.

[14] Y. Shen, A review on hydrothermal carbonization of biomass and plastic wastes to energy products, Biomass Bioenergy 134 (2020), https://doi.org/10.1016/j.biombioe.2020.105479.

[15] N.T. Machado, D.A.R. de Castro, M.C. Santos, M.E. Araújo, U. Lüder, L. Herklotz, M. Werner, J. Mumme, T. Hoffmann, Process analysis of hydrothermal carbonization of corn Stover with subcritical H2O, J. Supercrit. Fluids 136 (2018) 110–122, https://doi.org/10.1016/j.supflu.2018.01.012.

[16] J.G. Lynam, M.T. Reza, W. Yan, V.R. Vásquez, C.J. Coronella, Hydrothermal carbonization of various lignocellulosic biomass, Biomass Convers. Biorefinery. 5 (2015) 173–181, https://doi.org/10.1007/s13399-014-0137-3.

[17] Q. Wu, S. Yu, N. Hao, T. Wells, X. Meng, M. Li, Y. Pu, S. Liu, A.J. Ragauskas, Characterization of products from hydrothermal carbonization of pine, Bioresour. Technol. 244 (2017) 78–83, https://doi.org/10.1016/j.biortech.2017.07.138.

[18] A. Kruse, D. Baris, N. Tröger, P. Wieczorek, Scale-Up in Hydrothermal

Carbonization, Sustainable Carbon Materials from Hydrothermal Processes, John Wiley & Sons, Ltd, 2013, pp. 341–353.
[19] Dieter Wurz, Vorrichtung und Verfahren zur Behandlung von Biomasse, 2012. EP13005962.9A.
[20] M. Hitzl, A. Corma, F. Pomares, M. Renz, The hydrothermal carbonization (HTC) plant as a decentral biorefinery for wet biomass, Catal. Today 257 (2015) 154–159, https://doi.org/10.1016/j.cattod.2014.09.024.
[21] P. Burguete, A. Corma, M. Hitzl, R. Modrego, E. Ponce, M. Renz, Fuel and chemicals from wet lignocellulosic biomass waste streams by hydrothermal carbonization, Green Chem. 18 (2016) 1051–1060, https://doi.org/10.1039/c5gc02296g.
[22] S.K. Hoekman, A. Broch, C. Robbins, B. Zielinska, L. Felix, Hydrothermal carbonization (HTC) of selected woody and herbaceous biomass feedstocks, Biomass Conversion and Biorefinery 3 (2013) 113–126, https://doi.org/10.1007/s13399-012-0066-y.
[23] T. Fukuoka, Numerical analysis of a reactive extrusion process. Part II: simulations and verifications for the twin screw extrusion, Polym. Eng. Sci. 40 (2000) 2524–2538, https://doi.org/10.1002/pen.11383.
[24] S. Choulak, F. Couenne, Y. Le Gorrec, C. Jallut, P. Cassagnau, A. Michel, Generic dynamic model for simulation and control of reactive extrusion, Ind. Eng. Chem. Res. 43 (2004) 7373–7382, https://doi.org/10.1021/ie0342964.
[25] B. Vergnes, F. Berzin, Modeling of reactive systems in twin-screw extrusion: challenges and applications, C. R. Chim. 9 (2006) 1409–1418, https://doi.org/10.1016/j.crci.2006.07.006.
[26] T. Goma-Bilongo, F. Couenne, C. Jallut, Y. Le Gorrec, A. Di Martino, Dynamic modeling of the reactive twin-screw corotating extrusion process: experimental validation by using inlet glass fibers injection response and application to polymers degassing, Ind. Eng. Chem. Res. 51 (2012) 11381–11388, https://doi.org/10.1021/ie300698k.
[27] J. Grimard, L. Dewasme, A.V. Wouwer, A review of dynamic models of Hot-melt extrusion, Process 4 (2016), https://doi.org/10.3390/pr4020019.
[28] M. Wright, R.C. Brown, Establishing the optimal sizes of different kinds of biorefineries, Biofuel Bioprod. Biorefining. 1 (2007) 191–200, https://doi.org/10.1002/bbb.25.
[29] S. Bertolucci, B. Bressan, F. Caspers, Y. Garb, A. Gross, S. Pauletta, The BGU/CERN Solar Hydrothermal Reactor, 2014.
[30] P. Khongkrapan, T. Chinpensawat, Solar Energy-Assisted Activated Carbon Production, 2018. Melbourne, Australia.
[31] G. Ischia, M. Orlandi, M.A. Fendrich, M. Bettonte, F. Merzari, A. Miotello, L. Fiori, Realization of a solar hydrothermal carbonization reactor: a zero-energy technology for waste biomass valorization, J. Environ. Manag. 259 (2020), https://doi.org/10.1016/j.jenvman.2020.110067.
[32] J. Gómez-Hernández, P.A. González-Gómez, J.V. Briongos, D. Santana, Technical feasibility analysis of a linear particle solar receiver, Sol. Energy 195 (2020) 102–113, https://doi.org/10.1016/j.solener.2019.11.052.
[33] A. Sánchez-González, J. Gómez-Hernández, Beam-down linear Fresnel reflector: BDLFR, Renew. Energy 146 (2020) 802–815, https://doi.org/10.1016/j.renene.2019.07.017.
[34] S.K. Hoekman, A. Broch, L. Felix, W. Farthing, Hydrothermal carbonization (HTC) of loblolly pine using a continuous, reactive twin-screw extruder, Energy Convers. Manag. 134 (2017) 247–259, https://doi.org/10.1016/j.enconman.2016.12.035.
[35] K. Xu, M. Du, L. Hao, J. Mi, Q. Yu, S. Li, A review of high-temperature selective absorbing coatings for solar thermal applications, J. Materiomics. 6 (2020) 167–182, https://doi.org/10.1016/j.jmat.2019.12.012.
[36] A.Y. Krylova, V.M. Zaitchenko, Hydrothermal carbonization of biomass: a review, Solid Fuel Chem. 52 (2018) 91–103, https://doi.org/10.3103/S0361521918020076.
[37] K. Tekin, S. Karagöz, S. Bektaş, A review of hydrothermal biomass processing, Renew. Sustain. Energy Rev. 40 (2014) 673–687, https://doi.org/10.1016/j.rser.2014.07.216.
[38] H.B. Sharma, A.K. Sarmah, B. Dubey, Hydrothermal carbonization of renewable waste biomass for solid biofuel production: a discussion on process mechanism, the influence of process parameters, environmental performance and fuel properties of hydrochar, Renew. Sustain. Energy Rev. 123 (2020), https://doi.org/10.1016/j.rser.2020.109761.
[39] M. Heidari, O. Norouzi, S. Salaudeen, B. Acharya, A. Dutta, Prediction of hydrothermal carbonization with respect to the biomass components and severity factor, Energy Fuels 33 (2019) 9916–9924, https://doi.org/10.1021/acs.energyfuels.9b02291.
[40] T. Rogalinski, T. Ingram, G. Brunner, Hydrolysis of lignocellulosic biomass in water under elevated temperatures and pressures, J. Supercrit. Fluids 47 (2008) 54–63, https://doi.org/10.1016/j.supflu.2008.05.003.
[41] J. Stemann, A. Putschew, F. Ziegler, Hydrothermal carbonization: process water characterization and effects of water recirculation, Bioresour. Technol. 143 (2013) 139–146, https://doi.org/10.1016/j.biortech.2013.05.098.
[42] M. Jatzwauck, A. Schumpe, Kinetics of hydrothermal carbonization (HTC) of soft rush, Biomass Bioenergy 75 (2015) 94–100, https://doi.org/10.1016/j.biombioe.2015.02.006.
[43] M.T. Reza, W. Yan, M.H. Uddin, J.G. Lynam, S.K. Hoekman, C.J. Coronella, V.R. Vásquez, Reaction kinetics of hydrothermal carbonization of loblolly pine, Bioresour. Technol. 139 (2013) 161–169, https://doi.org/10.1016/j.biortech.2013.04.028.
[44] C. Kersting, J. Prüss, H. Warnecke, Residence time distribution of a screw-loop reactor: experiments and modeling, Chem. Eng. Sci. 50 (1995) 299–308, https://doi.org/10.1016/0009-2509(94)00236-K.
[45] R.W. Nachenius, T.A. Van De Wardt, F. Ronsse, W. Prins, Residence time distributions of coarse biomass particles in a screw conveyor reactor, Fuel Process. Technol. 130 (2015) 87–95, https://doi.org/10.1016/j.fuproc.2014.09.039.
[46] D.A. Sievers, J.J. Stickel, Modeling residence-time distribution in horizontal screw hydrolysis reactors, Chem. Eng. Sci. 175 (2018) 396–404, https://doi.org/10.1016/j.ces.2017.10.012.
[47] R. Baron, P. Vauchel, A. Arhaliass, Modeling of twin-screw reactive extrusion: application to alginate extraction, IFAC Proc. Vol. (IFAC-PapersOnline). 43 (2010) 341–346, https://doi.org/10.3182/20100707-3-BE-2012.0094.
[48] K. Lachin, Z. Youssef, G. Almeida, P. Perré, D. Flick, Residence time distribution analysis in the transport and compressing screws of a biomass pretreatment process, Chem. Eng. Res. Des. 154 (2020) 162–170, https://doi.org/10.1016/j.cherd.2019.12.011.
[49] J.Y. Jang, M.M. Khonsari, S. Bair, On the elastohydrodynamic analysis of shear-thinning fluids, Proc. R. Soc. A Math. Phys. Eng. Sci. 463 (2007) 3271–3290, https://doi.org/10.1098/rspa.2007.0062.
[50] O. Levenspiel, Tracer Technology Modeling the Flow of Fluids, 2012.
[51] H.F. Giles, J.R. Wagner, E.M. Mount, 17 - shear rate, pressure drop, and other extruder calculations, Extrusion (2005) 161–163, https://doi.org/10.1016/B978-081551473-2.50018-0.
[52] M. Pecchi, F. Patuzzi, D. Basso, M. Baratieri, Enthalpy change during hydrothermal carbonization of biomass: a critical review, J. Therm. Anal. Calorim. 141 (2020) 1251–1262, https://doi.org/10.1007/s10973-019-09117-4.
[53] W. Yan, J.T. Hastings, T.C. Acharjee, C.J. Coronella, V.R. Vásquez, Mass and energy balances of wet torrefaction of lignocellulosic biomass, Energy Fuels 24 (2010) 4738–4742, https://doi.org/10.1021/ef901273n.
[54] L. Levine, S. Levine, Chapter 11 - scale-up, experimentation, and data evaluation, Extrusion Cooking (2020) 331–389, https://doi.org/10.1016/B978-0-12-815360-4.00011-0.
[55] Hoyt C. Hottel, Adel F. Sarofim, Radiative Transfer, 1967.
[56] I.H. Bell, J. Wronski, S. Quoilin, V. Lemort, Pure and pseudo-pure fluid thermophysical property evaluation and the open-source thermophysical property library coolprop, Ind. Eng. Chem. Res. 53 (2014) 2498–2508, https://doi.org/10.1021/ie4033999.
[57] S. Guo, X. Dong, T. Wu, C. Zhu, Influence of reaction conditions and feedstock on hydrochar properties, Energy Convers. Manag. 123 (2016) 95–103, https://doi.org/10.1016/j.enconman.2016.06.029.
[58] C. He, C. Tang, C. Li, J. Yuan, K. Tran, Q. Bach, R. Qiu, Y. Yang, Wet torrefaction of biomass for high quality solid fuel production: a review, Renew. Sustain. Energy Rev. 91 (2018) 259–271, https://doi.org/10.1016/j.rser.2018.03.097.